Modern Physics Letters A

IMPLEMENTATION OF THE CMS-HIG-18-011 ANALYSIS IN THE MADANALYSIS 5 FRAMEWORK

JOON-BIN LEE

Department of Physics and Astronomy, Seoul National University, Gwanak-ro 1, Gwanak-gu Seoul, 08826, South Korea

joon.bin.lee@cern.ch

JEHYUN LEE

Department of Physics and Astronomy, Seoul National University, Gwanak-ro 1, Gwanak-gu Seoul, 08826, South Korea

leejs9125@gmail.com

Received (Day Month Year)
Revised (Day Month Year)

We present the implementation in the MadAnalysis 5 framework of the CMS-HIG-18-011 search for exotic decays of the Standard Model Higgs boson, in which the Higgs boson is assumed to decay into a pair of light pseudoscalar a_1, that then further decay into a di-muon and di-b-jet final state. This analysis considers proton-proton collisions at a centre-of-mass energy of 13 TeV and data collected by the CMS experiment in 2016, with an integrated luminosity of 35.9 fb^{-1}. We present a selection of recast predictions, obtained with MadAnalysis 5 and Delphes 3, that include a few differential distributions, yields and efficiencies. We show that they agree at a level of a few percents with public CMS results.

1. Introduction

In this note, we describe the validation of our reimplementation, in the MadAnalysis 5 framework [1–4], of the CMS-HIG-18-011 search [5] for exotic decays of the Standard Model Higgs boson into a pair of light pseudoscalar particles a_1, where one of the pseudoscalar decays to a pair of opposite-sign muons and the other one decays into a pair of b-quarks. This analysis focuses on 13 TeV LHC data and an integrated luminosity of 35.9 fb^{-1}.

The considered exotic decay of the Higgs boson is predicted in a variety of models, including the next-to-minimal supersymmetric extension of the Standard Model (NMSSM) [6], as well as models with additional scalar doublet and singlet (2HDM+S) [7–9]. To validate our reimplementation, we focus on an NMSSM setup in which one decouples most particles, except for the above-mentioned pseudoscalar states. Such a scenario has been studied in particular in the CMS-HIG-18-011 anal-

ysis that we reimplemented in this work.

In the rest of this note, we present a brief description of the CMS-HIG-18-011 analysis in section 2. Section 3 consists in the core of our work, and contains extensive information about the validation of our reimplementation. In particular, the presence of two b-jets in the final state makes this analysis particularly sensitive to the exact details of the b-jet identification algorithm. However, the b-jet identification efficiency provided by the CMS collaboration is not sufficient for a precise enough modeling in DELPHES 3. The method that we used to model in an accurate manner the CMS b-tagging algorithm is therefore explained in details in Section 3.2. We summarise our work and results in section 4.

2. Description of the analysis

The CMS-HIG-18-011 analysis performs a search for the Higgs boson decay chain $h \to a_1 a_1 \to \mu^+\mu^- b\bar{b}$. This analysis hence targets a final state containing two opposite-sign muons and two b-tagged jets. In the next subsection, we present the definition of the muon and jet candidates that are used in this analysis, as well as the preselection cuts of the analysis. Then, in Section 2.2, we explain the event selection requirements leading to a good background rejection while preserving as many expected signal events as possible.

2.1. *Object definitions and preselection*

This analysis requires the presence of at least two final-state muons and two final-state b-jets. Two oppositely charged muons are required to conservatively satisfy an online selection based on the CMS muon triggering system. This enforces that the final state includes two muons with a transverse momentum $p_T > 17$ GeV (leading muon μ_1) and 8 GeV (subleading muon μ_2). Moreover, the geometrical limitations of the CMS muon system leads to the following extra requirements on the muon's p_T and pseudorapidities η,

$$p_T(\mu_1) \ > \ 20 \text{ GeV} \ , \ p_T(\mu_2) \ > \ 9 \text{ GeV} \ \text{ and } \ |\eta(\mu_{1,2})| \ < \ 2.4. \tag{1}$$

Additionally, a particle-flow-based relative isolation is enforced. This requires that the sum of the transverse energy of any detector-level object present in a cone of radius $R = 0.4$ centered on the muon is smaller than 0.15 times the muon p_T^μ,

$$I_{rel} = \frac{1}{p_T^\mu} \sum_i (p_T)_i < 0.15. \tag{2}$$

The CMS-HIG-18-011 analysis moreover targets a signal scenario in which the narrow width approximation is valid for the new pseudoscalar a_1, and its mass is considered to fulfil 20 GeV $\leq m_{a_1} \leq$ 62.5 GeV. The invariant mass of the two-muon system is, therefore, restricted to lie within a slightly wider mass range,

$$19.5 \text{ GeV} \ < m_{\mu\mu} \ < \ 63.5 \text{ GeV}. \tag{3}$$

Jets are reconstructed by clustering detector-level objects with the anti-k_T algorithm [10] with a distance parameter of 0.4. The transverse momentum p_T and pseudorapidity (η) of the leading jet j_1 and subleading jets j_i (with $i \neq 1$) are imposed to satisfy

$$p_T(j_1) \ > \ 20 \text{ GeV}, \ p_T(j_i) > 15 \text{ GeV and } |\eta(j_{1,i})| \ < \ 2.4. \tag{4}$$

Events must contain at least two jets, with the leading two jets have to be well separated from the selected muons in the transverse plane, by a distance $\Delta R > 0.5$. b-tagging makes use of the CSVv2 algorithm [11] that relies on secondary vertex information. One of the jets must satisfy tight working point criteria, whereas another one has to satisfy loose working point requirements. The misidentification rate of light jets as b-jets is in average of 10% (0.1%) for the tight (loose) working point, the one of c-jets as b-jets is of 30% (2%), for a tagging efficiency of about 80% (40%). If there are more than two b-jets in the event, the two with the largest p_T are considered as originating from a pseudoscalar a_1 decay.

Finally, the missing transverse momentum vector $\mathbf{p_T^{miss}}$ is defined as the opposite of the vector sum of the momentum of all reconstructed physics object candidates, and the missing transverse energy is defined by the norm of this vector,

$$E_T^{miss} = |\mathbf{p_T^{miss}}|. \tag{5}$$

2.2. *Event Selection*

Following the preselection described in the previous section, signal events are subjected to additional selection cuts to minimise the Standard Model background contamination. As the transverse momentum of the neutrinos arising from semi-leptonic B-hadron decays is small, we require,

$$E_T^{miss} \ < \ 60 \text{ GeV}. \tag{6}$$

Next, as both the muons and b-jets are the decay products of a pseudoscalar boson a_1, one requires that the values of the invariant mass of dimuon system ($m_{\mu\mu}$) and the one of the two-b-jet system (m_{bb}) are close to each other. Therefore, the relative difference between these two invariant masses is evaluated through a quantity χ_{bb} defined by

$$\chi_{bb} \ = \ \frac{(m_{bb} - m_{\mu\mu})}{\sigma_{bb}}, \tag{7}$$

where σ_{bb} is a mass resolution associated with the reconstruction of the two-b-jet system. The invariant mass of the whole system comprising those four objects ($m_{\mu\mu bb}$) should moreover be compatible with the Higgs-boson mass m_h. One subsequently defines the relative difference χ_h,

$$\chi_h \ = \ \frac{(m_{\mu\mu bb} - m_h)}{\sigma_h}, \tag{8}$$

Fig. 1. Feynman diagrams illustrating the two hard process considered in the event generation processes relevant for the validation of the implementation in the MadAnalysis 5 framework of the CMS-HIG-18-011 analysis. The signal comprises a gluon fusion component (left) and vector-boson fusion component (right).

where σ_h is the mass resolution associated with the reconstruction of the Higgs boson candidate ($\mu\mu bb$). Events are selected by requiring that the squared sum of these two variables, $\chi^2 = \chi^2_{bb} + \chi^2_h$, is smaller than 5,

$$\chi^2 \ < \ 5. \tag{9}$$

3. Validation

3.1. *Event generation*

In order to generate events necessary to valide our implementation, we use the NMSSMHET simplified model [9]. The latter involves two free parameters, the mass of pseudoscalar m_{a_1} and tanβ, that is defined as the ratio of the vacuum expectation values of the two Higgs doublets of the model. tanβ moreover that determines the branching fraction of the a_1 boson to Standard Model particles. Following the CMS-HIG-18-011 analysis and the corresponding publicly available validation material, tanβ is set to 2 and we consider three pseudoscalar mass points,

$$m_{a_1} = 20,\ 40,\ 60 \text{ GeV}. \tag{10}$$

As there is no strong dependence of the branching ratio $\mathcal{B}(a_1 \to b\bar{b})$ and $\mathcal{B}(a_1 \to \mu^+\mu^-)$ on m_{a_1} [9], the total signal cross section defined as the product of the Standard Model Higgs boson production cross section (σ_h) and the relevant branching fractions is set to a constant value,

$$\sigma_h \times \mathcal{B}(h \to a_1 a_1 \to \mu^+\mu^- b\bar{b}) \approx 8 \text{ fb}. \tag{11}$$

We generate 1,000,000 events for each test sample. In order to mimic CMS signal event generation (so that we could compare our predictions to public material), we consider Higgs boson production via gluon fusion and vector boson fusion, as illustrated by the two Feynman diagrams shown in Figure 1. The total production cross sections resulting from a leading-order (LO) calculation achieved within the MadGraph5_aMC@NLO [12] framework and that are used for our signal normalisation, are, for each of the two subprocesses, 48.58 pb and 3.78 pb respectively.

The generation of the hard process is performed by using the NMSSMHET model implementation [9] in the UFO format [13], that can be used with the MadGraph5_aMC@NLO framework [12] at LO in QCD. Our matrix elements are

convoluted with the NNPDF3.0 set of parton densities [14], and the Pythia 8.212 package [15] with the CUETP8M1 tune [16] is used to model parton showering and hadronisation.

The simulation of the response of the CMS detector is based on the Delphes 3 program [17], which internally relies on Fastjet [18] for object reconstruction. We start from the default CMS detector parametrisation and then impose modifications as follows.

First, the mimimum p_T thresholds for muons and jets are reduced to 5 and 10 GeV respectively, in order to cover the full signal region.

Second, the muon and jet reconstruction efficiencies contained in the Run II CMS card in Delphes version 3.4.2 cannot cover such small p_T region. Therefore, they are extrapolated from the default ones to conservatively accept all objects used in this analysis.

Finally, the b-jet identification efficiencies based on the CSVv2 algorithm [11], which is used in CMS-HIG-18-011 analysis, have a large dependence on the jet transverse momentum. However, only average efficiency values are provided by the CMS collaboration. To approximatively model the p_T dependence of the combined secondary vertex algorithm used in this work, we have used the efficiency functions associated with the loose working point of the deep combined secondary vertex (DeepCSV) algorithm described in the CMS b-jet identification paper [11]. These are then re-weighted via the average tagging efficiencies of the CSVv2 algorithm, as further described in the next section. This re-weighting method has the great advantage of reflecting not only the overall b-tagging power of the CSVv2 algorithm, but also the p_T dependence of this general CMS b-tagging algorithm.

3.2. *Refinements of our event selection*

This work uses the same event selection as described in Section 2. However, additional details are necessary to reproduce the CMS-HIG-18-011 results. This section first describes the re-weighting method that we used to improve the modeling of the b-tagging performance in Delphes 3, and then explains how to estimate the mass resolutions σ_{bb} and σ_h that are needed to calculate the χ_{bb} and χ_h quantities of Section 2.

As noted in Section 3.1, the HIG-18-011 analysis used the CSVv2 b-tagging algorithm. The average efficiencies and mistagging rates of this algorithm are provided in the CMS b-jet identification publication [11], but there is no information about their p_T dependence. We have however found out that ignoring this p_T dependence can make a difference of about 20 % in the final results.

To recover this, we assume that the p_T dependence of the DeepCSV and CSVv2 algorithms is similar. This assumption is justified as both methods use an almost identical approach based on combined information originating from displaced tracks and secondary vertices. We hence implement the publicly available loose b-tagging efficiency and mis-tagging rates of the DeepCSV algorithm in Delphes 3, with their

full dependence on the jet's transverse momentum. In a second step, we re-weight the generated events to account for the different average efficiencies associated with the loose working points of the DeepCSV and CSVv2 algorithms. In practice, we use as a re-weghting factor the squared ratio of the p_T-independent efficiencies, $(\bar{\epsilon}_L^{v2}/\bar{\epsilon}_L^{D})^2$, where $\bar{\epsilon}_L^{v2}$ and $\bar{\epsilon}_L^{D}$ are respectively the CSVv2 and DeepCSV algorithm efficiencies as provided in the CMS b-tagging performance publication [11].

At last, the signal region event selection requires that at least one jet passes the requirement of the tight b-jet discriminator. The final event weight is therefore calculated as

$$w = \left(\frac{\bar{\epsilon}_L^{v2}}{\bar{\epsilon}_L^{D}}\right)^2 \cdot \left[1 - \left(1 - \frac{\epsilon_T^{v2}(j_i)}{\epsilon_L^{v2}(j_i)}\right) \cdot \left(1 - \frac{\epsilon_T^{v2}(j_j)}{\epsilon_L^{v2}(j_j)}\right)\right]. \tag{12}$$

In this equation, $\epsilon_{T(L)}^{v2}(j_i)$ represents the efficiency that the i^{th} jet (j_i) satisfies the tight (loose) CSVv2 selection criteria, that we estimate again from DeepCSV public information,

$$\epsilon_{T,L}^{v2}(j_i) = \frac{\bar{\epsilon}_{T,L}^{v2}}{\bar{\epsilon}_{T,L}^{D}} \cdot \epsilon_{T,L}^{D}(j_i). \tag{13}$$

Here, $\epsilon_{T,L}^{D}(j_i)$ are the DeepCSV tight and loose p_T-dependent efficiencies.

After the signal region selection of two jets and two muons, the mass resolutions of the di-b-jet (σ_{bb}) and reconstructed Higgs boson candidate (σ_h) are estimated by fitting the corresponding invariant-mass distributions with Gaussian functions. However, the CMS analysis note does not provide the exact values of these resolutions as obtained from the fit. We have therefore estimated these values by performing our own fit of the invariant-mass distributions.

As a rough approximation, we estimate the input values of the mass resolutions σ_{bb}^i and σ_h^i that are used in our Gaussian fitting procedure from the muon and jet p_T resolutions of the CMS detector. Each muon and jet originating from the Higgs boson decay has an average transverse momentum of about 30 GeV. The momentum resolution of a 30 GeV muon is expected to be of about 1% [19], whereas that of a 30 GeV jet is expected to be of about 17% [20]. Based on these values, the initial input mass resolution of the di-b-jet system is set to $\sigma_{bb}^i = 0.17 m_{a_1}$, and the one of the reconstructed Higgs boson candidate is fixed to $\sigma_h^i = 9.3$ GeV. Our Gaussian fitting is then performed within a fitting range of $m_{a_1(h)} \pm 1.5\sigma_{bb(h)}^i$ from the above input values.

Figure 2 and 3 show the invariant-mass distributions of the di-b-jet system and of the reconstructed Higgs boson candidate, together with the corresponding Gaussian fit results. The average mass resolution of the di-b-jet system is found to be $0.173 m_{a_1}$, whilst that of the Higgs boson candidate is equal to 9.66 GeV. As a result, the χ_{bb}, χ_h and $\chi^2 = \chi_{bb}^2 + \chi_h^2$ quantities can be calculated by using eqs. (7) and (8).

In the left panel of Figure 4, we show the χ^2 distribution that is obtained after applying all selections except the $\chi^2 < 5$ cut. The results are presented for a scenario

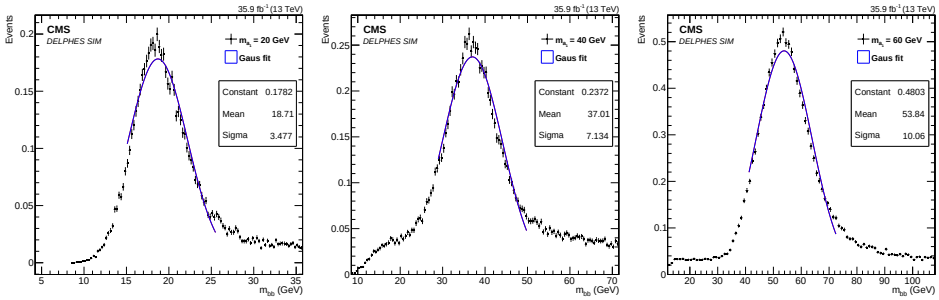

Fig. 2. The di-b-jet invariant-mass distribution with its Gaussian fitting, for pseudoscalar mass scenarios of $m_{a_1} = 20$ (left), 40 (center), and 60 (right) GeV.

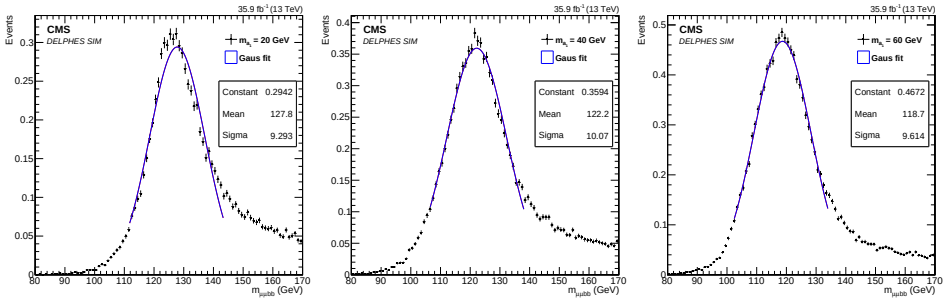

Fig. 3. The invariant-mass distribution of the reconstructed Higgs boson candidate, with its Gaussian fitting for pseudoscalar mass scenarios of $m_{a_1} = 20$ (left), 40 (center), and 60 (right) GeV.

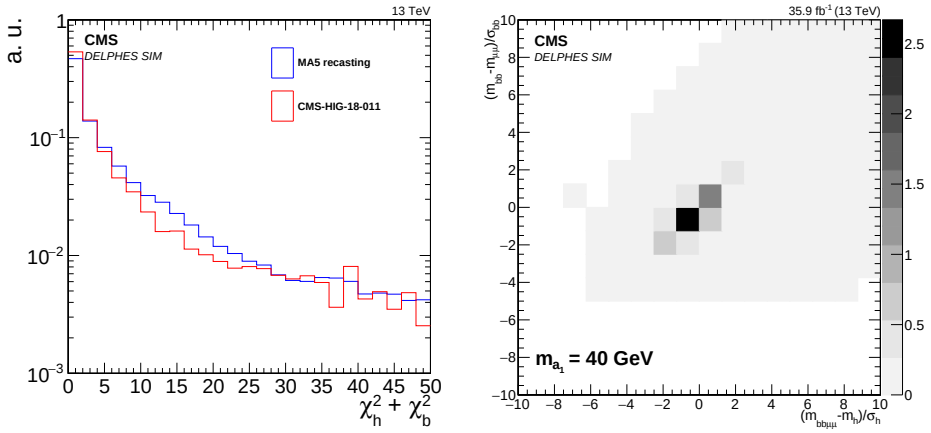

Fig. 4. **Left:** The χ^2 distribution associated with the scenario in which $m_{a_1} = 40$ GeV, once all analysis selections except the $\chi^2 < 5$ requirement are applied. **Right:** Two-dimensional distribution of the $(m_{bb} - m_{\mu\mu})/\sigma_{bb}$ and $(m_{\mu\mu bb} - 125\ \text{GeV})/\sigma_h$ quantities for the same scenario and after applying all the cuts of the analysis with the exception of the $\chi^2 < 5$ requirement.

Table 1. Event yields resulting from the object selection of Section 2.1 (the so-called $\mu^+\mu^- b\bar{b}$ selection) and after the final selection cuts presented in Section 2.2. The results are normalised to an integrated luminosity of 35.9 fb^{-1}. We moreover include the total event selection efficiencies (ϵ) for three mass scenarios. We compare predictions obtained with MadAnalysis 5 and the public CMS results.

		$\mu^+\mu^- b\bar{b}$ selection	Final selection	ϵ (%)
$m_{a_1} = 20$ GeV	CMS-HIG-18-011	14.0 ± 0.1	6.0 ± 0.1	42.9
	MA5 Recasting	13.2	5.6	42.5
	Difference δ (%)	5.7	6.7	0.4
$m_{a_1} = 40$ GeV	CMS-HIG-18-011	14.8 ± 0.1	7.5 ± 0.1	50.7
	MA5 Recasting	15.9	7.4	46.2
	Difference δ (%)	7.4	1.3	4.5
$m_{a_1} = 60$ GeV	CMS-HIG-18-011	16.7 ± 0.1	10.1 ± 0.1	60.5
	MA5 Recasting	16.9	10.1	60.0
	Difference δ (%)	1.2	0.3	0.5

in which the mass of the pseudoscalar a_1 is fixed to 40 GeV. In the right panel of the figure, we moreover show the two-dimensional distribution of the χ_{bb} and χ_h quantities for the same scenario and after applying again all analysis cuts but the last one. This illustrates the quality of our fit and its impact on the signal reconstruction.

3.3. *Comparison with official results*

To validate our results, we compare predictions obtained with our MadAnalysis 5 implementation (and our tuned detector simulation based on Delphes 3) to the CMS official results presented in the CMS-HIG-18-011 analysis note for the three considered new physics scenarios. As a first test, we compare the curve shown in the left panel of Figure 4 to the first figure (Fig. 1) of the CMS note. The shape of the two distributions are similar, the values in the most populated first bins being found to differ by at most a few percent. We additionally compare the shape of the contours shown in the right panel of Figure 4 with the one exhibited in the second figure (Fig. 2) of the CMS publication. Here, the central bin are even populated equally. As already mentioned in the previous section, this validates our fitting procedure.

In Table 1, we compare CMS public yields with the recasting results predicted with MadAnalysis 5 after the object definition selection of Section 2.1, *i.e.* before applying the $p_T^{miss} < 60$ GeV and $\chi^2 < 5$ requirements, and after the full analysis selection. The differences between the CMS and MadAnalysis 5 event yields

($N^{\rm CMS}$ and $N^{\rm MA5}$) is quantified through relative differences,

$$\delta = \frac{|N^{\rm CMS} - N^{\rm MA5}|}{N^{\rm CMS}} \tag{14}$$

Overall results agree at the level of the few percent, where the best agreement is achieved for the final selection with the 60 GeV pseudoscalar mass scenario which only shows a 0.3 % difference with the CMS-HIG-18-011 results from Ref. 5. Event selection efficiencies (ϵ) and the corresponding differences are also computed. The level of agreement between the CMS results and the MadAnalysis 5predictions is again found to lie at the percent level.

Although the event yields exhibit a larger difference after the object definition selection (ranging up to 7.4% for the $m_{a_1} = 40$ GeV scenario), we consider that such a feature should be expected as resulting from our approximate modeling of the p_T dependence of the b-tagging performance. Such an order of magnitude is indeed typical from the differences originating from the use of the DeepCSV and CSVv2 algorithms. We nevertheless consider this as a minor effect stemming from the lack of public knowledge about the new b-tagging algorithms used by CMS.

Even after adding the impact of our method to estimate the mass resolutions used in the CMS-HIG-18-011 analysis, only a small difference between MadAnalysis 5 predictions and CMS official results remains. We take it as sufficiently acceptable to guarantee the validation of our recast. Unfortunately, our validation cannot be performed further because of the lack of available public information.

4. Conclusion

In this note, we have documented a recast in the MadAnalysis 5 frsmework of the CMS-HG-18-011 search for light pseudoscalar particles originating from an exotic decay of the Standard Model Higgs boson. This search considers a final state comprising two b-jets and a pair of opposite-sign muons, and an integrated luminosity of 35.9 fb^{-1} of data collected at a centre-of-mass energy of 13 TeV.

Our work features two important differences with respect to what CMS has done. First, due to the lack of public knowledge about the transverse momentum dependence on the CSVv2 b-tagging algorithm performances, we have modeled our b-tagging efficiencies and mistagging rates in Delphes 3 by using the dependence of the DeepCSV algorithm performances on the transverse momentum of the jets. We have moreover included an event reweighting procedure dealing with the differences between the average tagging efficiencies of the two algorithms. Second, we had to implement our own Gaussian fitting procedure to recover the invariant-mass resolutions expected from the signal, in the case of the reconstructed Higgs boson and pseudoscalar boson a_1. These are extensively detailed in Section 3.2.

To validate our reimplementation of the above search, we generated three signal samples in accordance with the CMS prescriptions. We have found that our approximate treatment of the mass resolutions and the CMS b-tagging performance are reasonable enough. These has allowed us to obtained an agreement with the CMS

results at the level of a few percent. In contrast, only a poor level of agreement of about 20% can be reached without implementing our two classes of changes.

Subsequently to the lack of public CMS information for this analysis, we have only validated our code by comparing a few differential distributions and event yields at two stages of the full event selection. Our results exhibit a reliable agreement at the percent level. The implemented code is available online from the MadAnalysis 5 dataverse [21], at https://doi.org/10.14428/DVN/UOH6BF, which also includes the cards and UFO model that have been used in our validation procedure.

References

1. E. Conte, B. Fuks and G. Serret, *Comput. Phys. Commun.* **184**, 222 (2013), arXiv:1206.1599 [hep-ph].
2. E. Conte, B. Dumont, B. Fuks and C. Wymant, *Eur. Phys. J. C* **74**, 3103 (2014), arXiv:1405.3982 [hep-ph].
3. B. Dumont, B. Fuks, S. Kraml, S. Bein, G. Chalons, E. Conte, S. Kulkarni, D. Sengupta and C. Wymant, *Eur. Phys. J. C* **75**, 56 (2015), arXiv:1407.3278 [hep-ph].
4. E. Conte and B. Fuks, *Int. J. Mod. Phys. A* **33**, 1830027 (2018), arXiv:1808.00480 [hep-ph].
5. CMS Collaboration, A. M. Sirunyan *et al.*, *Phys. Lett. B* **795**, 398 (2019), arXiv:1812.06359 [hep-ex].
6. U. Ellwanger, C. Hugonie and A. M. Teixeira, *Phys. Rept.* **496**, 1 (2010), arXiv:0910.1785 [hep-ph].
7. M. Dine, W. Fischler and M. Srednicki, *Phys. Lett. B* **104**, 199 (1981).
8. J. E. Kim and H. P. Nilles, *Phys. Lett. B* **138**, 150 (1984).
9. D. Curtin *et al.*, *Phys. Rev. D* **90**, 075004 (2014), arXiv:1312.4992 [hep-ph].
10. M. Cacciari, G. P. Salam and G. Soyez, *JHEP* **04**, 063 (2008), arXiv:0802.1189 [hep-ph].
11. CMS Collaboration, A. Sirunyan *et al.*, *JINST* **13**, P05011 (2018), arXiv:1712.07158 [physics.ins-det].
12. J. Alwall, R. Frederix, S. Frixione, V. Hirschi, F. Maltoni, O. Mattelaer, H. S. Shao, T. Stelzer, P. Torrielli and M. Zaro, *JHEP* **07**, 079 (2014), arXiv:1405.0301 [hep-ph].
13. C. Degrande, C. Duhr, B. Fuks, D. Grellscheid, O. Mattelaer and T. Reiter, *Comput. Phys. Commun.* **183**, 1201 (2012), arXiv:1108.2040 [hep-ph].
14. NNPDF Collaboration, R. D. Ball *et al.*, *JHEP* **04**, 040 (2015), arXiv:1410.8849 [hep-ph].
15. T. Sjöstrand, S. Ask, J. R. Christiansen, R. Corke, N. Desai, P. Ilten, S. Mrenna, S. Prestel, C. O. Rasmussen and P. Z. Skands, *Comput. Phys. Commun.* **191**, 159 (2015), arXiv:1410.3012 [hep-ph].
16. CMS Collaboration, V. Khachatryan *et al.*, *Eur. Phys. J. C* **76**, 155 (2016), arXiv:1512.00815 [hep-ex].
17. DELPHES 3 Collaboration, J. de Favereau, C. Delaere, P. Demin, A. Giammanco, V. Lemaître, A. Mertens and M. Selvaggi, *JHEP* **02**, 057 (2014), arXiv:1307.6346 [hep-ex].
18. M. Cacciari, G. P. Salam and G. Soyez, *Eur. Phys. J. C* **72**, 1896 (2012), arXiv:1111.6097 [hep-ph].
19. CMS Collaboration, S. Chatrchyan *et al.*, *JINST* **7**, P10002 (2012), arXiv:1206.4071 [physics.ins-det].

20. CMS Collaboration, V. Khachatryan *et al.*, *JINST* **12**, P02014 (2017), arXiv:1607.03663 [hep-ex].
21. J.-B. Lee and J. Lee, *https://doi.org/10.14428/DVN/UOH6BF* (2020).